Journal of Sound and Vibration 329 (2010) 3065–3081

Contents lists available at ScienceDirect

Journal of Sound and Vibration

journal homepage: www.elsevier.com/locate/jsvi

Analytical predictions for vibration phase shifts along fluid-conveying pipes due to Coriolis forces and imperfections

Jon Juel Thomsen *, Jonas Dahl

Department of Mechanical Engineering, Technical University of Denmark, Building 404, DK-2800 Lyngby, Denmark

ARTICLE INFO

Article history:
Received 16 June 2009
Received in revised form
5 February 2010
Accepted 7 February 2010
Handling Editor: A.V. Metrikine
Available online 1 March 2010

ABSTRACT

Resonant vibrations of a fluid-conveying pipe are investigated, with special consideration to axial shifts in vibration phase accompanying fluid flow and various imperfections. This is relevant for understanding elastic wave propagation in general, and for the design and trouble-shooting of phase-shift measuring devices such as Coriolis mass flowmeters in particular. Small imperfections related to elastic and dissipative support conditions are specifically addressed, but the suggested approach is readily applicable to other kinds of imperfection, e.g. non-uniform stiffness or mass, non-proportional damping, weak nonlinearity, and flow pulsation. A multiple time scaling perturbation analysis is employed for a simple model of an imperfect fluid-conveying pipe. This leads to simple analytical expressions for the approximate prediction of phase shift, providing direct insight into which imperfections affect phase shift, and in which manner. The analytical predictions are tested against results obtained by pure numerical analysis using a Galerkin expansion, showing very good agreement. For small imperfections the analytical predictions are thus comparable in accuracy to numerical simulation, but provide much more insight. This may aid in creating practically useful hypotheses that hold more generally for real systems of complex geometry, e.g. that asymmetry or non-proportionality in axial distribution of damping will induce phase shifts in a manner similar to that of fluid flow, while the symmetric part of damping as well as non-uniformity in mass or stiffness do not affect phase shift. The validity of such hypotheses can be tested using detailed fluid-structure interaction computer models or laboratory experiments.

1. Introduction

An important quantity characterizing elastic wave propagation is the *phase shift* in oscillation between any two points of the medium. We present a systematic perturbation approach for deriving analytical expressions that relate phase shift to parameters characterizing vibrating pipes conveying fluid flow and possible imperfections. This is relevant to gain further insight into which factors influence phase shift and how, and for applications such as the design and troubleshooting of Coriolis mass flowmeters, where the primary quantity measured is phase shift.

Fluid flowing in a vibrating pipe prevents standing flexural waves, and thus there will be a shift in vibration phase (different from 0, π) between the transverse vibrations of any two pipe points, with a corresponding shift in zero-crossing times. Under certain conditions the phase shift is approximately proportional to mass flow, a property utilized with

* Corresponding author.
E-mail address: jjt@mek.dtu.dk (J.J. Thomsen).

0022-460X/$ - see front matter © 2010 Elsevier Ltd. All rights reserved.
doi:10.1016/j.jsv.2010.02.010

Coriolis mass flowmeters. But phase shifts could be influenced by a number of factors other than mass flow, e.g. non-proportional damping (which includes asymetric or nonlinear damping), nonlinearity (e.g. in pipe restraints and excitation coils), and various imperfections such as non-ideal boundary supports, rapid or resonant flow pulsation, and non-uniform flow profile or density. Some imperfections may be stationary in time, and can be compensated for by calibration. Other may fluctuate unobserved in time or space, impossible or impractical to control; they will reflect as apparent changes in mass flow, i.e. as erroneous flowmeter readings.

Using finite element methods [1–3], detailed computational models of real flowmeters can be set up that could possibly simulate any thinkable system specification and operating condition, and thus predict phase shifts. Simulation of detailed models may provide much data, but typically very little useful insight into basic dependencies. It is difficult to generalize the results beyond the particular parameters and conditions simulated; in this respect computer simulation parallels laboratory experiments. Furthermore, with 2D or 3D models, nonlinearity, nonstationarity, or full fluid–structure interaction taken into account, computational times may prohibit parameter-dependencies to be explored in any depth. Thus greatly simplified models, and approximate analysis that allows for more general conclusions, may provide direct insight, and help increasing the benefit of costly simulation and laboratory experiments.

We suggest using greatly simplified mathematical models of Coriolis flowmeters, along with systematic perturbation analysis, to asses how various factors could possibly influence phase shift and thus flowmeter output. We show how simple analytical expressions can be derived that relates phase shift to fluid mass flow, and to imperfections like non-ideal boundary supports and non-uniform distribution of stiffness (or mass) and damping. This is done for a simple model of straight single-tube pipe flowmeter, on the assumption that the effects are basically similar for more complicated geometries, and that results based on simple models are either directly transferable, or can be used for creating hypotheses that can be tested against full computational models or laboratory experiments. The model used in this study includes just of few imperfections, but effects of other kinds of perturbation could be analyzed along similar tracks. For example, we present a simple analytical prediction showing that any asymmetry in the structural damping of rotational motions at the flowmeter supports changes the measured phase shift in a manner indistinguishable from that caused be fluid flow. This means that any departure from perfect damping symmetry—perhaps fluctuating in time with other factors such as temperature or vibration—could be erroneously interpreted as a change in mass flow. Also, a small flexibility at a support ideally supposed to be rigid is predicted to increase the phase shift in linear proportion to the total support flexibility.

The vibrations of fluid-conveying pipes have been actively investigated for more than six decades [4,5], and some of this work is motivated by Coriolis flowmetering applications. Of the latter, many publications provide valuable analyses on how mass flow and also imperfections influence phase shift, see, e.g. the rather recent overview by Anklin et al. [6]. Any kind of imperfection has the potential to violate the assumed simple proportionality between mass flow and phase shift, or the independent determination of mass flow (from time shift) and fluid density (from change in resonance frequency). Imperfections can be features not accounted for in typical modeling (e.g. flow compressibility [7], damping [3,8,9], external vibrations [10], flexible supports, or nonlinearity), or features in a range not accounted for (e.g. large flow rates [11]), or features calling for higher modeling dimensionality (e.g. non-uniform flow profile [12]). Some works examine the effects of flexible supports on vibrations, but without consideration to fluid flow [13], or with consideration to fluid flow but not to phase shift [14–16]. Raszillier and Durst [17] used a perturbation-like approach to derive analytical expressions for the phase shift for fluid-conveying pipes, but did not consider imperfect supports. Effects of imperfect supports on phase shift have been studied using numerical solutions for a simple model [18,19]. The results of [19] suggest that any asymmetry in rotational damping at supports implies a phase shift similar to that of fluid flow; a similar effect of non-proportional damping was reported for a simple FEM model of a curved tube flowmeter [8]. Several studies derive analytical or semi-analytical predictions for phase shifts in the context relevant here. Typically the analytical expressions are for the ideal case [17], or are given not directly in terms of physical parameters but in terms of pipe motions or mode shapes (may depend non-trivially on physical parameters), or in terms of parameters determined only by numerical solutions of eigenvalue problems [20,21], or the results are not tested against numerical simulation or laboratory experiments. Kutin and Bajsić [9] derive analytical phase shift expressions taking into account imperfections in the form of small damping (though only uniformly distributed), axial force, and added mass, and show the predictions to agree with numerical solutions. The approximations are made by linearizing the effects of imperfections near the "perfect" case. This approach is appealing, appears simpler than the one described in the present work, and may be used for other imperfections as well. However, it assumes the pipe response to be simply time-harmonic in the drive frequency, and thus cannot be generalized to incorporate, e.g. nonlinearity, flow pulsations, or external disturbances at frequencies other than the drive frequency. Also, it does not provide a systematic and generalizable way of handling imperfections, such as the standard perturbation approach used here.

With the present work we present, exemplify, and test a systematic approach for the derivation of simple approximate analytical expression for phase shifts of pipe vibrations caused by fluid flow and various imperfections, using simplified models of real flowmeters. A summary of the model and the main results was presented in [22], while here we intend to provide sufficient detail for the analysis to appear self-contained. Section 2 presents the mathematical model of a fluid-conveying pipe, with small imperfections related to boundary supports and pipe uniformity. Section 3 presents a multiple scales perturbation analysis, employed directly to the partial differential equation of pipe motion, for calculating the response at primary resonance. This leads to simple analytical expressions for features that are important for applications,

such as changes in natural frequency and phase shifts between transverse vibrations at two points of the pipe axis. Section 4 describes how a standard Galerkin expansion was employed to calculate "exact" numerical solutions, for testing the accuracy of approximate analytical predictions. Section 5 demonstrates, by four examples, how the rather general analytical expression for phase shift derived in Section 3 can be used to investigate specific effects, and also tests the quality of the predictions against numerical analysis. Section 6 resumes the main results and their possible applicability.

2. Mathematical model

Fig. 1(a) shows a simple model of what will be referred to as the *ideal* fluid-conveying pipe. This pipe is straight, uniform, undamped, and perfectly hinged at the two supports, and the fluid flows uniformly at constant velocity and density. Fig. 1(b) shows the same pipe with some minor modifications, which we consider as *imperfections* of the ideal pipe: finitely small distributed transverse and rotational stiffness and damping, and finitely small support flexibility (i.e. finitely large support stiffness). Many other kinds of imperfections could be relevant, but to highlight the approach for examining effects of imperfections, we focus here on just a few. Also, the particular support conditions are chosen for convenience of illustrating the approach and interpretation of results, rather than for their relevance for applications; any other kind of supports could be chosen, as long as their "imperfection" with respect to an ideal support is small, i.e. the supporting reaction force to translation or rotation should be either very small or very large, corresponding to small or vanishing stiffness or flexibility, respectively.

The equation of motion governing transverse vibrations of the pipe can be derived using Newton's second and third law for, respectively, the external and internal forces on a differential pipe and fluid element, or by using Hamilton's principle, starting from expressions for the total energy and the work performed by non-conservative forces; see, e.g. [1,3,5,17] for details of derivation. The result can be written in the following nondimensional form (similar to what can be found, e.g. in [3,9]):

$$\ddot{u}+u''''+\varepsilon[\alpha(2v\dot{u}'+v^2u''+\dot{v}u')+L_ku+L_\beta\dot{u}]=\varepsilon p\delta(x-x_p)\cos(\Omega t), \tag{1}$$

where $u=u(x,t)$ is the transverse deflection from the static equilibrium $u=0$, $x\in[0;1]$ is the axial coordinate, L_k and L_β are linear spatial differential operators for describing arbitrarily distributed damping and (additional) stiffness:

$$L_k=k_u(x)-\frac{\mathrm{d}}{\mathrm{d}x}\left(k_\theta(x)\frac{\mathrm{d}}{\mathrm{d}x}\right),\quad L_\beta=\beta_u(x)-\frac{\mathrm{d}}{\mathrm{d}x}\left(\beta_\theta(x)\frac{\mathrm{d}}{\mathrm{d}x}\right), \tag{2}$$

the boundary conditions are

$$u+\varepsilon\pi^{-3}\kappa_{u0}u'''=u''=0\quad\text{for } x=0,$$

$$u-\varepsilon\pi^{-3}\kappa_{ul}u'''=u''=0\quad\text{for } x=1, \tag{3}$$

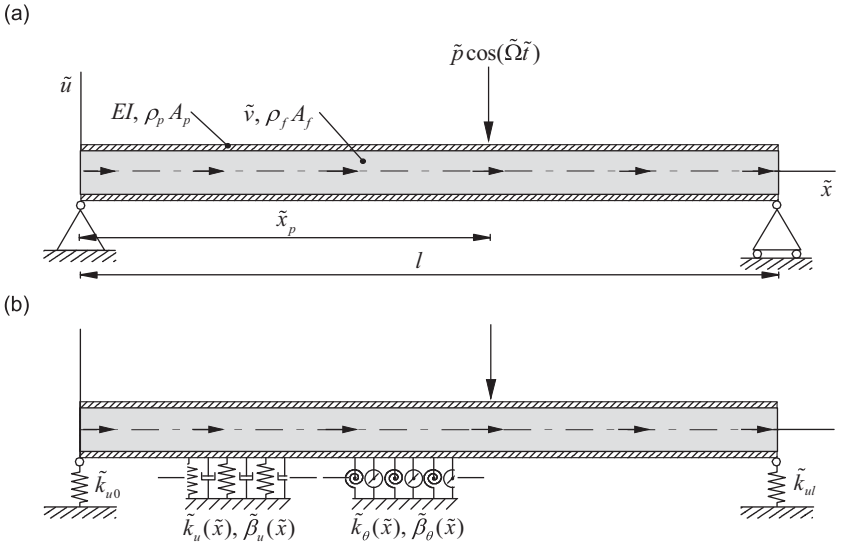

Fig. 1. Simple model of a transversly vibrating fluid-conveying pipe. (a) Ideal system; (b) with some imperfections: finitely small distributed transverse and rotational stiffness and damping, and finitely small support flexibility (i.e. finitely large support stiffness).

and all parameters, variables, and functions are nondimensional.

$$x=\tilde{x}/l,\quad u=\tilde{u}/l,\quad t=\tilde{\omega}\tilde{t},\quad \tilde{\omega}=\sqrt{EI/\rho Al^4},\quad v=\tilde{v}/\tilde{\omega}l,\quad \rho A=\rho_p A_p+\rho_f A_f,$$

$$\alpha=\rho_f A_f/\rho A,\quad \kappa_{u0,l}=48\pi^3 EI/\tilde{k}_{u0,l}l^3,\quad p=\tilde{p}/\rho Al\tilde{\omega}^2,\quad \Omega=\tilde{\Omega}/\tilde{\omega},$$

$$k_u=\tilde{k}_u/\rho A\tilde{\omega}^2,\quad k_\theta=\tilde{k}_\theta/\rho Al^2\tilde{\omega}^2,\quad \beta_u=\tilde{\beta}_u/\rho A\tilde{\omega},\quad \beta_\theta=\tilde{\beta}_\theta/\rho Al^2\tilde{\omega}. \tag{4}$$

In (1)–(4) a tilde denotes a corresponding physical variable or parameter, time t is nondimensionalized by the characteristic frequency $\tilde{\omega}$, the axial coordinate x and transverse deflection u by the pipe length l, flow speed v by the characteristic wave speed $\tilde{\omega}l$, ρA denotes mass per unit length (subscript p/f indicating pipe/fluid), EI is the flexural pipe stiffness per unit length, $\alpha\in[0;1[$ is the ratio of fluid mass to total mass, the functions $k_{u,\theta}(x)$ and $\beta_{u,\theta}(x)$ for $x\in[0;1]$ describe the (possibly non-uniform or discontinuous) axial distribution of, respectively, stiffness (additional to that of the ideal pipe), and viscous damping per unit pipe length (subscript u/θ indicating transverse/rotational), p is the amplitude of the time-harmonic excitation force at $x=x_p$ having normalized frequency Ω, κ_{u0} and κ_{ul} are the normalized transverse flexibilities of the boundary supports at $x=0$ and l, $\delta(x)$ is Dirac's delta function, dots and primes denote differentiation wrt. t and x, respectively, and ε is a bookkeeping parameter used for marking terms that are assumed to be small compared to other terms.

In (1)–(4) all terms multiplied by ε are assumed to be small, compared to the other terms. The parameter ε has no physical interpretation, but serves the purpose of "magnitude bookkeeping" through the different stages of analysis, explicitly quantifying the assumed order of magnitude of terms. In the final application of analysis results, we just substitute an ε-marked quantity (e.g. εp or $\varepsilon\alpha v$) by its specific value (e.g. p or αv), knowing that this value should be small in magnitude compared to unity for the results to be accurate, or at least that the corresponding term in the equation of motion should be small compared to terms not multiplied by ε. Thus the magnitude ordering in (1)–(4) implies the system to be basically a simply supported uniform pipe, with some minor additions or "imperfections" which are detailed further below. This implies considerable computational convenience, and is physically realistic for applications such as Coriolis flowmetering: The excitation p is weak (being resonant, not much is needed), the flow speed v is much smaller than what could cause buckling of the pipe, and changes only little over each period of pipe oscillation, the slopes u' are small, as is the non-uniformity in pipe stiffness L_k, the damping L_β, and the flexibility of supports $\kappa_{u0,l}$.

The detailed assumptions for (1)–(4) are the following: The pipe is considered a slender beam of uniform cross section and near-uniformly distributed flexural stiffness and mass, only transverse deflections in the plane of the excitation force are important, and the deflection slopes during vibrations are small, $(u')^2\ll 1$ The fluid inside the pipe is incompressible, and flows towards $x=1$ with a flat ("plug flow") velocity profile, i.e. $(v\rho_f A_f)'=0$ so that $v'=0$, and $v>0$. For the following analysis of (1)–(4) it assumed that the damping coefficients β_u and β_θ are small, as are the coefficients k_u and k_θ defining additional non-uniform stiffness, the transverse support flexibilities κ_{u0} and κ_{ul}, and the external forcing amplitude p (since the pipe is supposed to be driven at resonance). The flow speed is "small" in the sense that $|\tilde{v}|\ll\tilde{\omega}l$, i.e. a fluid particle travels only a small fraction of pipe length during each (characteristic) oscillation period $2\pi/\tilde{\omega}$, so that $0<v\ll 1$. All these assumptions hold approximately for applications such as Coriolis flowmetering under normal operating conditions. In this study we assume further that the flow speed changes only little during each transverse oscillation of the pipe, i.e. $v=v(\varepsilon t)$. For Coriolis flowmetering this assumption is adequate under typical operating conditions, but can be violated by the presence of flow pulsations in resonance with the pipe or rapid flow transients [23,24]; such cases are investigated separately [25]. For the boundary conditions (3), all terms proportional to products of small quantities (such as, e.g. $k_\theta\kappa_{u0}u'$) are considered $O(\varepsilon^2)$ and are consequently ignored compared to terms of order ε^0 and ε^1.

The first two terms in (1) represent, respectively, transverse inertia of the pipe and fluid, and flexural stiffness of the pipe. The third and fourth terms represent inertia forces of the Coriolis ($\varepsilon 2\alpha v\dot{u}'$) and centrifugal ($\varepsilon\alpha v^2u''$) type; they are due to the fluid flowing at speed v through pipe segments of instantaneous curvature radius $1/u''$, rotating at angular velocity $\dot{u}'$. Terms similar to these occur in numerous pipe-flow studies (e.g. [5,17]). The fifth term ($\varepsilon\alpha\dot{v}u'$) represents the effect of time-varying flow speed, as is relevant, e.g. with pulsating flow or flow transients. The three terms depending on flow velocity v arise when calculating the transverse fluid acceleration $\ddot{u}_f$ at axial coordinate x: On the assumptions made, any fluid particle moves inside the pipe in a trajectory $(x_f,y_f)=(x_f(t),u(x_f(t),t)$, where $\mathrm{d}x_f/\mathrm{d}t=v$. At pipe axial coordinate x the transverse fluid velocity is then $\dot{u}_f=(\partial u/\partial x)(\mathrm{d}x_f/\mathrm{d}t)+\partial u/\partial t=vu'+\dot{u}$, i.e. given by the material derivative $v\partial/\partial x+\partial/\partial t$ of u. The transverse acceleration of the fluid particle is similarly given by the material derivative of $\dot{u}_f$, giving $\ddot{u}_f=\ddot{u}+2v\dot{u}'+v^2u''+(\dot{v}+vv')u'$, where the term with v' vanishes due to the assumption of flow incompressibility and uniform cross section. Multiplying $\ddot{u}_f$ by the mass of the fluid element gives the resulting transverse force at the fluid element, which in turn must equal the reaction force from the pipe.

The functions $k_{u,\theta}(x)$ and $\beta_{u,\theta}(x)$ can be used to include any kind of *small* non-uniformity in linear stiffness and dissipation. These functions do not have to be continuous in x, and can thus model also stiffness or damping distributions confined to only finite parts of pipe length, or (using Dirac delta functions $\delta(x-x_j)$) at certain isolated points $x=x_j$, which can even be at the pipe supports (i.e. $x_j\to\{0_+,1_-\}$). Small support *flexibility*—i.e. large but finite support stiffness—is instead represented by the flexibility coefficients κ_{u0} and κ_{ul} in the boundary condition (3); this allows the imperfectly rigid supports to be described in terms of *small* perturbations to the ideal supports. The scaling of flexibility coefficients in (4) implies that when the pipe vibrates harmonically in a fundamental mode, then κ_{u0} or κ_{ul} roughly equals the vibration

amplitude at a flexible support in ratio to the midpipe transverse vibration amplitude; for example, $\kappa_{u0}=0.1$ means that the flexibility of the left pipe support allows it to vibrate at an amplitude about 10 percent of the midpipe vibration amplitude in the fundamental mode.

To illustrate the smallness of the third term in (1) for applications such as Coriolis flowmetering, we note that in that case the dominating motion of the pipe model can be roughly estimated as $u(x,t)=A\sin(\pi^2 t)\sin(\pi x)$, where A is the (controlled) vibration amplitude, and π^2 is the natural frequency corresponding to the fundamental symmetric vibration mode $\sin(\pi x)$. It then follows that the ratio of the Coriolis acceleration $2\alpha v\dot{u}'$ in (1) to the transverse acceleration $\ddot{u}$ has magnitude $2\pi^{-1}\alpha v$, while the similar ratio for the centripetal acceleration $\alpha v^2 u''$ is $\pi^{-2}\alpha v^2$. For an example industrial Coriolis flowmeter (Siemens SITRANS FC300 DN4) measuring water flow, one finds $\alpha=0.29$ while at full nominal rate (350 kg/h) $v=0.65$; this gives Coriolis and centripetal acceleration ratios of, respectively, 0.12 and 0.012, which would be even smaller at non-maximal flow rates.

Recapping that in this study an ideal pipe has no transverse or rotational damping ($\beta_u=\beta_\theta=0$), no inhomogeneity in transverse or flexural stiffness ($k_u=k_\theta=0$), and no transverse flexibility at either support end ($\kappa_{u0}=\kappa_{ul}=0$), we next calculate the dynamic response of the imperfect pipe, considering this as a slight perturbation of the response of the ideal pipe.

3. Primary resonant response I: analytical prediction using perturbation analysis

3.1. Method

The equation of motion (1)–(3) is a linear partial differential equation with homogeneous boundary conditions. A solution $u(x,t)$ is sought that is approximately valid under the assumptions stated above, and which can be used for setting up a simple analytical prediction for the difference $\Delta\psi$ in vibration phase measured between two symmetric pipe points $x_{1,2}=\frac{1}{2}\mp\Delta x$, $\Delta x\in]0;\frac{1}{2}[$. This phase shift, or the corresponding time shift in velocity zero-crossing, is the quantity actually measured in Coriolis flowmetering. For manufacturers, it is of interest to be able to predict how the phase shift depends on physical parameters such as flow speed and system imperfections, and to know the accuracy of the prediction.

The aim is here at transparent analytical expressions, allowing for direct insight into the effects of primary physical parameters on phase shift. Thus semi-analytical methods which give the phase shift in terms of quantities requiring numerical solutions, such as, e.g. the exact natural frequencies and mode shapes of the imperfect pipe, will not suffice. Neither will methods that do not consider the forced response, but instead calculate the free vibration modes of the imperfect pipe, and then *assume* the forced response to be in a particular mode, uninfluenced by other modes; such an assumption does not hold generally, e.g. when nonlinearity, flow pulsation, or external vibrations are involved.

For certain kinds of imperfection a simple perturbation method will work, e.g. the authors initially used the Lindstedt–Poincaré method (both in its standard form, and in the Rayleigh–Schrödinger variant [26] which is particularly convenient here) to produce simple analytical predictions of phase shifts for the case $L_k=L_\beta=\kappa_{u0}=\kappa_{ul}=0$, which agreed closely with numerical simulation. However, in search for a generally applicable technique that can readily be adapted to investigate other kinds of imperfections for fluid-conveying pipes [22,25], choice fell on the more powerful though also more elaborate *method of multiple scales* [26–29], which can readily handle, e.g. nonlinearity, or even excitation with random components [30].

3.2. General approximate solution in terms of slowly varying amplitudes

Using the method of multiple scales, we search for a perturbation solution in form of a two-time scale expansion valid for $\varepsilon\ll 1$:

$$u(x,t)=u_0(x,T_0,T_1)+\varepsilon u_1(x,T_0,T_1)+O(\varepsilon^2), \tag{5}$$

where $T_0=t$ and $T_1=\varepsilon t$, i.e. T_1 is a slow timescale, and $O(\varepsilon^n)$ denotes terms of order of magnitude ε^n and smaller. Inserting into (1)–(3) and balancing terms of like powers of ε one obtains, to lowest order ε^0, a partial differential equation with boundary conditions for u_0:

$$D_0^2 u_0+u_0''''=0 \quad \text{for } x\in]0;1[, \tag{6}$$

$$u_0=u_0''=0 \quad \text{for } x\in\{0,1\}, \tag{7}$$

and to first order ε^1, an equation for u_1:

$$D_0^2 u_1+u_1''''=-2D_0D_1u_0-\alpha(2vD_0u_0'+v^2u_0'')-L_ku_0-L_\beta(D_0u_0)+p\delta(x-x_p)\cos(\Omega T_0), \quad x\in]0;1[, \tag{8}$$

with boundary conditions:

$$u_1+\kappa_{u0}\pi^{-3}(u_1'''+u_0''')=0 \quad \text{and} \quad u_1''=0 \quad \text{for } x=0,$$

$$u_1-\kappa_{ul}\pi^{-3}(u_1'''+u_0''')=0 \quad \text{and} \quad u_1''=0 \quad \text{for } x=1, \tag{9}$$

where the operator $D_i^j=\partial^j/\partial T_i^j$ denotes partial differentiation of order j wrt. T_i.

Consistently with the physical assumptions underlying the magnitude ordering of terms in (1)–(3), the small effects of flow speed, damping, stiffness non-uniformity, external excitation, and support flexibility first appears at the ε^1-level of approximation (8) and (9), which determines the first-order correction u_1 to the dominating component of motion u_0.

For cases violating the assumption (cf. Section 2) of slowly changing flow speed $v=v(\varepsilon t)$, a term $\alpha(D_0 v)u_0'$ subtracts from the right-hand side of (8). Also, the terms in (9) with u_1''' might seem to belong to the second order ε^2-level, which is ignored in the present analysis, and thus for consistency should be ignored at the ε^1-level (9) of boundary conditions. However, with u_0 describing motions in the primarily excited fundamental mode φ_{01}, and u_1 mainly describing motions of the flow-excited mode φ_{02}, the higher wavenumber of φ_{02} implies that the magnitude of u_1''' is not necessarily small compared to u_0''', even if u_1 is small compared to u_0. The inclusion of the u_1'''-terms in (9) adds only little to the computational burden, while in the case of flexible supports ($\kappa_{u0}+\kappa_{ul}\neq 0$) substantially improving the quality of the analytical predictions at the ε^1-level (because it allows for a small but important rigid-body correction to the second-mode vibration component in u_1).

The general solution to (6) and (7) can be expressed as a series expansion in terms of a set of mode shape functions φ_{0j}:

$$u_0(x,T_0,T_1)=\sum_{j=1}^{\infty}A_{0j}(T_1)\varphi_{0j}(x)\mathrm{e}^{\mathrm{i}\omega_{0j}T_0}+cc, \tag{10}$$

where A_{0j} are complex-valued amplitude functions of slow time, i is the imaginary unit, cc denotes complex conjugates of the preceding terms, and ω_{0j} and $\varphi_{0j}(x)$ are, respectively, the linear natural frequencies and mode shapes for the unperturbed, ideal system ($\varepsilon=0$), i.e.:

$$\omega_{0j}=(j\pi)^2,\quad \varphi_{0j}(x)=\sqrt{2}\sin(j\pi x),\quad j=1,2,\ldots. \tag{11}$$

The latter satisfy the ordinary differential equation with boundary conditions for the free mode shapes, as well as orthogonality and normalization conditions, i.e.:

$$\varphi_{0j}''''=\omega_{0j}^2\varphi_{0j},$$

$$\varphi_{0j}(0)=\varphi_{0j}''(0)=\varphi_{0j}(1)=\varphi_{0j}''(1)=0,$$

$$\int_0^1\varphi_{0j}\varphi_{0k}\,\mathrm{d}x=\delta_{jk},\quad j,k=1,2,\ldots, \tag{12}$$

where δ_{jk} is Kronecker's delta, and the first index of φ, ω and A here and below indicates the level of approximation (e.g. φ_{0j} and A_{0j} are, respectively, mode shapes and amplitude functions for the lowest, unperturbed ε^0-level of approximation).

One can proceed with (10) as is, but since we are specifically considering pipes under resonant excitation at or near the fundamental natural frequency ω_{01}, it is adequate to retain only that corresponding part of (10), i.e. we let $A_{0j}=0$ for $j=2,3,\ldots$, so that

$$u_0(x,T_0,T_1)=A_{01}(T_1)\varphi_{01}(x)\mathrm{e}^{\mathrm{i}\omega_{01}T_0}+cc. \tag{13}$$

This describes the unperturbed motion of the pipe in its fundamental mode. The purpose of the perturbation analysis is then to calculate how the perturbations, i.e. the ε-terms in (1)–(3), will cause corrections to this fundamental motion, including contributions from modes higher than the first.

Inserting (13) into (8) and (9), the perturbation correction u_1 becomes governed by

$$D_0^2u_1+u_1''''=f_1(x,T_1,A_{01})\mathrm{e}^{\mathrm{i}\omega_{01}T_0}+cc, \tag{14}$$

where

$$f_1(x,T_1,A_{01})=-\mathrm{i}2\omega_{01}(D_1A_{01})\varphi_{01}-\alpha(\mathrm{i}2v\omega_{01}\varphi_{01}'+v^2\varphi_{01}'')A_{01}-(L_k\varphi_{01}+\mathrm{i}\omega_{01}L_\beta\varphi_{01})A_{01}+\tfrac{1}{2}p\delta(x-x_p)\mathrm{e}^{\mathrm{i}\sigma T_1}, \tag{15}$$

and the boundary condition (9) becomes

$$u_1+\pi^{-3}\kappa_{u0}u_1'''=\kappa_{u0}A_{01}\sqrt{2}\mathrm{e}^{\mathrm{i}\omega_{01}T_0}+cc\quad\text{and}\quad u_1''=0\quad\text{for } x=0,$$

$$u_1-\pi^{-3}\kappa_{ul}u_1'''=\kappa_{ul}A_{01}\sqrt{2}\mathrm{e}^{\mathrm{i}\omega_{01}T_0}+cc\quad\text{and}\quad u_1''=0\quad\text{for } x=1. \tag{16}$$

Here a detuning parameter σ has been introduced to quantify the nearness of the excitation frequency Ω to the fundamental, unperturbed natural frequency ω_{01}, i.e.:

$$\Omega=\omega_{01}+\varepsilon\sigma. \tag{17}$$

Eqs. (14) and (15) for u_1 is a linear partial differential equation with inhomogeneous terms (the right-hand side) which are harmonic in T_0. We seek a particular solution for u_1 in terms of a Galerkin-expansion of the n lowest unperturbed modes shapes φ_{0j}, i.e.:

$$u_1(x,T_0,T_1)=\left(A_{01}(T_1)\varphi_{101}(x)+\sum_{j=2}^{n}B_{1j}(T_1)(\varphi_{0j}(x)+\varphi_{10j}(x))\right)\mathrm{e}^{\mathrm{i}\omega_{01}T_0}+cc, \tag{18}$$

where $\varphi_{0j}(x)$ is given by (11), and $\varphi_{10j}(x)$ are rigid body modes (as indicated by an additional middle index of zero; the first index still refers to the order of approximation):

$$\varphi_{10j}(x)=\sqrt{2}j^3(\kappa_{u0}(1-x)-(-1)^j\kappa_{ul}x),\quad j=1,2,\ldots. \tag{19}$$

The rigid body modes (19) are non-zero only in the case of transverse support flexibility, $\kappa_{u0}+\kappa_{ul}\neq 0$, and along with (12) ensures (18) to satisfy the boundary conditions (16) for any set of yet unknown complex-valued functions $A_{01}(T_1)$ and $B_{1j}(T_1)$. Physically, the inclusion of rigid body modes in the set of expansion functions allows for a simple analytical approximation of transverse pipe deformations, when supports are not completely rigid. Alternatively, a new set of mode shapes φ_{0j} could be computed, taking into account support flexibility (by contrast to (11)); however, the expressions would be much more complicated, while not providing significant increase in accuracy for the assumed small support flexibility. Mathematically, the rigid body modes (19) were determined by substituting (18) into the boundary conditions (16), requiring φ_{10j} to be linear in x (the requirement for a rigid body mode), and solving for the linear coefficients. Note that the summing index in (18) starts at j=2, i.e. the basic mode φ_{01} is excluded from the expansion. This is not an assumption, but a restriction needed for the boundary conditions (16) to be fulfilled, reflecting that vibrations in the fundamental form φ_{01} are already taken into account at the ε^0-level through the function u_0, cf. (13).

Next, to obtain the functions B_{1j}, and thus u_1, we follow the standard Galerkin procedure and insert (18) into (14), multiply by any φ_{0s}, s=1,2,…,n, integrate over x, calculate the mode shape integrals using (11) and (12), and find

$$((\omega_{0j}/\omega_{01})^2-1)B_{1j}=R_{1j},\quad j=1,2,\ldots,n, \tag{20}$$

where

$$R_{1j}=\int_0^1\varphi_{0j}\left(\omega_{01}^{-2}f_1+A_{01}\varphi_{101}+\sum_{s=2}^{n}B_{1s}\varphi_{10s}\right)\mathrm{d}x. \tag{21}$$

With f_1 depending on $A_0(T_1)$ and its time-derivative D_1A_0, cf. (15), Eqs. (20) and (21) constitute n ordinary differential equations for the determination of the n unknown functions $A_{01}(T_1)$ and $B_{1j}(T_1)$, j=2,3,…,n. It appears from (20) and (21), and the definition of ω_{0j} in (11), that the first-order amplitude functions $B_{1j}(T_1)$ decrease rapidly in magnitude (roughly as j^{-4}) with the mode number j. Thus, aiming at a two-mode approximation to u_1, which will suffice to include all essential effects of concern in the present case of resonant excitation of the fundamental mode, we let n=2 in (20) and (21), and find for j=1 and 2, respectively,

$$\int_0^1\varphi_{01}(\omega_{01}^{-2}f_1+A_{01}\varphi_{101}+B_{12}\varphi_{102})\,\mathrm{d}x=0, \tag{22}$$

$$\int_0^1\varphi_{02}(\omega_{01}^{-2}f_1+A_{01}\varphi_{101}+B_{12}\varphi_{102})\,\mathrm{d}x=((\omega_{02}/\omega_{01})^2-1)B_{12}, \tag{23}$$

which should be solved for $A_{01}(T_1)$ and $B_{12}(T_1)$.

To relate to the typical application of the method of multiple scales, we note that (22) corresponds to a *solvability condition* [26,27]; its fulfillment ensures the solution u_1 to (14) be free of secular terms, i.e. terms proportional to $T_0\mathrm{e}^{\mathrm{i}\omega_{01}T_0}$, which would violate the initial assumption underlying (5) that $|\varepsilon u_1|\ll|u_0|$ at all times $T_0>0$. For the ideal case of no support flexibility ($\kappa_{u0}=\kappa_{ul}=0$) the rigid body components φ_{10j} vanish, and (22) reduces to $\int_0^1\varphi_{01}f_1\,\mathrm{d}x=0$, expressing the well-known [26] requirement for the existence of solutions to an inhomogeneous differential equation with a self-adjoint homogeneous differential operator: The inhomogeneous part (here f_1) must be orthogonal to the solution (here φ_{01}) of the corresponding homogeneous equation. With finite support flexibility ($\kappa_{u0}+\kappa_{ul}\neq 0$), the boundary conditions (16) imply that the operator for the homogeneous part of the system (14)–(16) is not self-adjoint, and thus the solvability condition (22) appears "non-standard". Often, with the method of multiple scales, a solvability condition is imposed directly, using explicit knowledge on what could cause secular terms; here it appears automatically, as a byproduct of the Galerkin discretization process.

In solving (22) and (23) for A_{01} and B_{12} we can make greatly simplifying approximations, consistent with the already established level of accuracy: It follows directly from (23) that

$$B_{12}=\frac{\frac{1}{15\pi^4}\int_0^1\varphi_{02}f_1\,\mathrm{d}x+\frac{1}{15}A_{01}\int_0^1\varphi_{02}\varphi_{101}\,\mathrm{d}x}{1-\frac{1}{15}\int_0^1\varphi_{02}\varphi_{102}\,\mathrm{d}x}, \tag{24}$$

where ω_{0j} from (11) has been substituted. Here the denominator is $O(1)$, while the second integral in the numerator, due to φ_{101}, is proportional to the small parameters κ_{u0} and κ_{ul}. For the first integral of the numerator it follows, when inserting (15) for f_1, that all terms are proportional to quantities assumed small (ν, L_k, L_β, p), except the first term which is of order unity. However, the integral of this first term vanishes due to the orthogonality of φ_{01} and φ_{02}, cf. (12), and B_{12} is thus proportional to the small parameters (as required also for u_1 to be small compared to u_0, cf. (18)). But this implies that the

third term in (22) is proportional to the *square* product of small parameters, and for consistency with the present first-order approximate analysis, such terms should be ignored compared to the first and second terms in (22) which are, respectively, $O(1)$ and proportional to the first power of the small parameters. As a result we can obtain A_{01} by solving (22) with the B_{12}-term ignored, i.e. the solvability condition becomes

$$\int_0^1 \varphi_{01}(\omega_{01}^{-2} f_1 + A_{01}\varphi_{101})\,\mathrm{d}x = 0. \tag{25}$$

Then (24) can be used to find B_{12} in terms of A_{01}, in all calculations keeping terms of the two largest orders of magnitude (e.g. $O(1)$ and $O(\varepsilon)$, *or* $O(\varepsilon)$ and $O(\varepsilon^2)$), and ignoring any higher.

Substituting φ_{02}, φ_{101}, φ_{102}, and f_1 from (11), (19), and (15) with (2) into (24), and performing the integrations, one finds B_{12} in terms of A_{01}:

$$B_{12} = \left(1+\frac{8}{15\pi}\kappa_1\right)\left[\frac{1}{15\pi^2}\left(\pi\kappa_2 - k_2 - i\left(\frac{16}{3}\alpha\nu+\beta_2\right)\right)A_{01} + \frac{1}{30\pi^4}p\varphi_{02}(x_p)\mathrm{e}^{\mathrm{i}\sigma T_1}\right], \tag{26}$$

where the first parenthesis results from Taylor-expanding the reciprocal of the denominator in (24) for small $\kappa_{u0,l}$, and the total support flexibility κ_1, the asymmetry κ_2 in support flexibility and the first-to-second mode coupling stiffness and damping constants k_2 and β_2 are defined by, respectively,

$$\kappa_1 = \kappa_{u0} + \kappa_{ul}, \quad \kappa_2 = \kappa_{u0} - \kappa_{ul},$$

$$k_2 = \frac{1}{\pi^2}\int_0^1 \varphi_{02}L_k\varphi_{01}\,\mathrm{d}x = \frac{1}{\pi^2}\int_0^1 (k_u\varphi_{01}\varphi_{02} + k_\theta\varphi_{01}'\,\varphi_{02}')\,\mathrm{d}x,$$

$$\beta_2 = \int_0^1 \varphi_{02}L_\beta\varphi_{01}\,\mathrm{d}x = \int_0^1 (\beta_u\varphi_{01}\varphi_{02} + \beta_\theta\varphi_{01}'\,\varphi_{02}')\,\mathrm{d}x, \tag{27}$$

where k_2 and β_2 have been calculated using (2), (12), and integration by parts.

For determining A_{01} we start by inserting (11), (15), and (19) into the solvability condition (25), calculate the mode shape integrals, and find

$$\mathrm{i}D_1A_{01} - \left(K_1 - \mathrm{i}\frac{1}{2}\beta_1\right)A_{01} = \frac{1}{4\pi^2}\varphi_{01}(x_p)p\mathrm{e}^{\mathrm{i}\sigma T_1}, \tag{28}$$

where the first-mode modal stiffness and damping constant k_1 and β_1, and the change in effective transverse stiffness K_1 due imperfections are defined by, respectively:

$$k_1 = \frac{1}{\pi^2}\int_0^1 \varphi_{01}L_k\varphi_{01}\,\mathrm{d}x = \frac{1}{\pi^2}\int_0^1 (k_u\varphi_{01}^2 + k_\theta\varphi_{01}'^2)\,\mathrm{d}x \geq 0,$$

$$\beta_1 = \int_0^1 \varphi_{01}L_\beta\varphi_{01}\,\mathrm{d}x = \int_0^1 (\beta_u\varphi_{01}^2 + \beta_\theta\varphi_{01}'^2)\,\mathrm{d}x \geq 0,$$

$$K_1 = \tfrac{1}{2}\alpha\nu^2 + \pi\kappa_1 - \tfrac{1}{2}k_1, \tag{29}$$

where k_1 and β_1 have been calculated using (2), (12), and integration by parts.

The presence of the operator D_1 makes (28) a first-order ordinary differential equation for the determination of $A_{01}(T_1)$. To solve it we express the complex-valued function $A_{01}(T_1)$ in polar form:

$$A_{01} = \tfrac{1}{2}a_{01}\mathrm{e}^{\mathrm{i}(\sigma T_1 - \eta_{01})}, \tag{30}$$

where $a_{01}=a_{01}(T_1)$ and $\eta_{01}=\eta_{01}(T_1)$ are real-valued functions. Substituting this into (28) gives, when separating real and imaginary parts, the corresponding equations for a_{01} and η_{01}:

$$D_1a_{01} = -\frac{1}{2}\beta_1a_{01} + \frac{1}{2\pi^2}\varphi_{01}(x_p)p\sin\eta_{01},$$

$$a_{01}D_1\eta_{01} = (\sigma + K_1)a_{01} + \frac{1}{2\pi^2}\varphi_{01}(x_p)p\cos\eta_{01}. \tag{31}$$

On the assumptions already stated, all terms on both right-hand sides are small, implying that also the rate of changes D_1a_{01} and $D_1\eta_{01}$ on the left-hand sides are small, so that $a_{01}(T_1)$ and $\eta_{01}(T_1)$, $T_1=\varepsilon t$, are indeed slowly varying functions of time.

Now we can calculate the two-mode ($n=2$) approximate pipe response $u(x,t)$. Using (5), (13), (17), (18), (26), (30), and the definitions under (5) of T_0 and T_1, and consistently ignoring terms of order ε^2 and smaller, it becomes

$$u(x,t) = a_{01}(t)[h_k(x)\cos(\Omega t - \eta_{01}) + h_\beta(x)\sin(\Omega t - \eta_{01})] + \varepsilon\frac{1}{15\pi^4}p\varphi_{02}(x_p)\varphi_{02}(x)\cos(\Omega t), \tag{32}$$

where

$$h_k(x) = \varphi_{01}(x) + \varepsilon\left(\varphi_{101}(x) + \frac{1}{15\pi^2}(\pi\kappa_2 - k_2)\varphi_{02}(x)\right),$$

$$h_\beta(x) = \varepsilon\frac{1}{15\pi^2}\left(\frac{16}{3}\alpha v + \beta_2\right)\left(\left(1 + \frac{8}{15\pi}\kappa_1\right)\varphi_{02}(x) + \varphi_{102}(x)\right), \tag{33}$$

and the slowly varying amplitude and phase functions (a_{01},η_{01}) are solutions of (31). The accuracy of this approximate solution assumes all terms multiplied by ε be small compared to unity.

3.3. Interpreting the general solution

Recalling that ε is the bookkeeper of terms assumed to be small, (32) and (33) shows that the pipe basically vibrates in its driven fundamental mode φ_{01}, i.e. $u \to u_0 = a_{01}\varphi_{01}\cos(\Omega t - \eta_{01})$ as $\varepsilon \to 0$. On top of this there are small additional motions—those multiplied by ε—accounting for the effects of mass flow αv, for possible external excitation of the second mode $p\varphi_{02}(x_p)$, and for the various imperfections considered.

The antisymmetric second mode φ_{02} is only excited if there are "asymmetrical causes", that is nonzero mass flow αv, or asymmetry in the damping or stiffness imperfections (i.e. nonzero κ_2, k_2, β_2), or asymmetrical external forcing (i.e. $x_p \neq \frac{1}{2}$ so that $\varphi_{02}(x_p) \neq 0$). The first rigid body mode φ_{101} is excited only if there is transverse support flexibility (i.e. $\kappa_{u0} + \kappa_{ul} \neq 0$, cf. (19)), while excitation of the second rigid body mode φ_{102} further requires mass flow αv or damping asymmetry β_2. Whatever mix of modes (φ_{10j}, φ_{0j}) are excited, every pipe point oscillates at a single frequency Ω, that of the excitation.

It readily appears from (32) and (33) that the part of the response u which is related to the flow and the damping (the term with $h_\beta(x)$) is phase-shifted 90° in time wrt. the response related to elastic stiffness (the term with $h_k(x)$). For an ideal pipe, the expressions for h_k and h_β in (33) reduce to $h_k = \varphi_{01}(x), h_\beta = \varepsilon(16/45\pi^2)\alpha v\varphi_{02}(x)$, i.e. the pipe vibrates in the resonantly excited fundamental symmetric mode φ_{01}, with a small overlay—proportional to mass flow αv—of vibrations of the antisymmetric second mode φ_{02}. Since the latter vibrates 90° out-of-phase wrt. the fundamental mode, the resulting motion u is a traveling wave, i.e. the nodes of the vibration pattern move in time, and different points on the pipe axis do not cross the equilibrium line $u = 0$ simultaneously.

For Coriolis flowmeters the time shift Δt in zero-crossing between two pipe axis points, or the corresponding phase shift $\Delta\psi = \Omega\Delta t$, is considered proportional to mass flow αv and thus—after suitable calibration—a measure of mass flow. However, as appears already from (32) and (33), various imperfections may induce time- or phase-shifts in a manner similar to that of mass flow. For example, in (32) and (33) the mass flow αv occurs only in summation with β_2, and thus the effect of mass flow and (asymmetric or non-proportional) damping on phase shift cannot be distinguished. If the part caused by damping is constant in time, this only implies a change of calibration offset and thus is not necessarily a problem for applications. But if the damping part is fluctuating in time, e.g. due to temperature changes, bubbles in the flow, or eddy current damping from magnets, then this would reflect as a phase shift and thus a meter reading of an equivalent change in mass flow, even at constant true mass flow.

Next the above results are used to set up simple predictions for vibration phase shift due to fluid flow and imperfections.

3.4. Main case of interest: phase shift under mid-pipe sharply resonant excitation

We specialize to the case of common interest with Coriolis flowmeters, where periodic excitation is usually applied mid-pipe, and maintained by feedback-control to be in sharp resonance with a fundamental, symmetric mode shape.

Eqs. (32) with (33) describe stationary as well as transient solutions to (1). Being particularly interested in the steady-state vibrations that remain when the effect of a disturbance (e.g. a change in mass flow or damping) has settled, we note that such solutions are characterized by having constant amplitude and phase, i.e. $a_{01}(T_1) = \tilde{a}_{01}$ and $\eta_{01}(T_1) = \tilde{\eta}_{01}$, and $D_1\tilde{a}_{01} = D_1\tilde{\eta}_{01} = 0$. Inserting this into (31) and solving the resulting algebraic equations gives

$$\tilde{a}_{01} = \frac{\frac{1}{2\pi^2}p\varphi_{01}(x_p)}{\sqrt{(\sigma + K_1)^2 + \frac{1}{4}\beta_1^2}}; \quad \tilde{\eta}_{01} = \arctan\left(\frac{-\frac{1}{2}\beta_1}{\sigma + K_1}\right). \tag{34}$$

We define *the resonant detuning* σ^* as the value of σ maximizing $\tilde{a}_{01}$ in (34), i.e.:

$$\sigma^* = -K_1. \tag{35}$$

According to (17) and (11) this corresponds to the excitation frequency $\Omega = \omega_{01}^*$,

$$\omega_{01}^* = \pi^2 - \varepsilon K_1, \tag{36}$$

which is then the fundamental resonance frequency of the pipe under fluid flow and in the presence of imperfections, differing a little (since εK_1 is small) from the unperturbed natural frequency ω_{01}. With K_1 defined by (29) it appears that ω_{01}^* decreases with the softening effects of mass flow (via αv^2) and support flexibility κ_1, but increases with the presence of additional transverse stiffness k_1. The corresponding resonant amplitude and phase is, by (34) and (35), and noting that the phase here is wrt. the excitation force p and independent of x:

$$\tilde{a}_{01}^* = \frac{p\varphi_{01}(x_p)}{\pi^2\beta_1}; \quad \tilde{\eta}_{01}^* = \frac{\pi}{2}. \tag{37}$$

With Coriolis flowmetering the excitation is maintained by feedback-control to be in sharp resonance with the fundamental mode, i.e. $\sigma=\sigma^*$, and thus $\Omega=\omega_{01}^*$ holds approximately on a timescale comparable to that of changes in flow speed or other parameters. Also, the excitation is usually applied mid-pipe, i.e. $x_p=\frac{1}{2}$, and the response is measured at two points symmetrically located around the mid-pipe, i.e. $x_{1,2}=\frac{1}{2}\mp\Delta x$, $\Delta x\in]0;\frac{1}{2}[$. Under such conditions we find, using (32), (37), (11), and trigonometric identities that

$$u(x,t) = \frac{\sqrt{2}}{\pi^2}\,\frac{p}{\beta_1}\sqrt{h_k(x)^2+h_\beta(x)^2}\,\sin(\omega_{01}^* t-\psi(x)), \tag{38}$$

where the phase ψ depends on x,

$$\psi(x) = \arctan\left(\frac{h_\beta(x)}{h_k(x)}\right) \approx \frac{h_\beta(x)}{h_k(x)}, \tag{39}$$

and the approximation for the last term is adequate under the already stated assumption on the smallness of quantities in h_β. The difference $\Delta\psi$ in phase between the two measurement points $x_{1,2}$ is

$$\Delta\psi(\Delta x) = \psi(\tfrac{1}{2}-\Delta x)-\psi(\tfrac{1}{2}+\Delta x), \tag{40}$$

and for further calculations it is useful to note from (11) and (19) that

$$\varphi_{01}(\tfrac{1}{2}\pm\Delta x) = \sqrt{2}\cos(\pi\Delta x),$$

$$\varphi_{02}(\tfrac{1}{2}\pm\Delta x) = \mp\sqrt{2}\sin(2\pi\Delta x),$$

$$\varphi_{10j}(\tfrac{1}{2}\pm\Delta x) = \sqrt{2}j^3(\kappa_{u0}(\tfrac{1}{2}\mp\Delta x)-(-1)^j\kappa_{ul}(\tfrac{1}{2}\pm\Delta x)), \quad j=1,2. \tag{41}$$

Finally insert (39) into (40) using (41), Taylor-expand $\Delta\psi$ under the stated assumption on the smallness of parameters, assume the measurement points $x_{1,2}$ are not close to the supports (i.e. Δx is away from $\frac{1}{2}$ so that $\sqrt{2}\cos(\pi\Delta x)$ is not small), and find the following simple prediction for the phase shift:

$$\Delta\psi(\Delta x) = s_1(\Delta x)(\alpha v+\tfrac{3}{16}\beta_2), \tag{42}$$

where

$$s_1(\Delta x) = \frac{64}{45\pi^2}\sin(\pi\Delta x)\left(1+\kappa_1\left(\frac{8}{15\pi}-\frac{1}{2\cos(\pi\Delta x)}\left(1-\frac{8\Delta x}{\sin(\pi\Delta x)}\right)\right)\right), \tag{43}$$

and for consistency in the approximation order, terms of the two lowest orders of magnitude are retained (e.g. αv, $\alpha v\kappa_1$, β_2, and $\beta_2\kappa_1$), while terms of higher order are neglected (e.g. $\alpha v\kappa_1^2$ and $\beta_2\kappa_1 k_2$).

Equivalently to the phase shift $\Delta\psi$, the time shift Δt between vibration properties (e.g. the zero-crossings of velocity) at the two measurement points is often used (e.g. [17]), differing from phase shift only by a constant of proportionality:

$$\Delta t(\Delta x) = \Delta\psi(\Delta x)/\omega_{01}^*. \tag{44}$$

It appears from (42) and (43) that s_1 is the *linear meter sensitivity*, i.e. the factor of proportionality between mass flow and phase shift for small mass flows. Letting $\alpha v=0$, the *zero shift* is obtained, i.e. the phase shift $\Delta\psi_0$ measured without any flow:

$$\Delta\psi_0(\Delta x) = \tfrac{3}{16}\beta_2 s_1(\Delta x). \tag{45}$$

Had (11) not been used already to substitute $\omega_{0j}=(j\pi)^2$, the factor $64/45\pi^2$ in (43) would appear instead as $64\pi^2/3(\omega_{02}^2-\omega_{01}^2)$, i.e. the meter sensitivity grows with the closeness between the natural frequency ($\approx\omega_{01}$) of the fundamental symmetric mode which is driven at resonance, and the natural frequency (ω_{02}) of the antisymmetric mode excited by the flow (sometimes called the *Coriolis frequency* and *Coriolis mode*, respectively); this agrees with a well-known observation in Coriolis flowmetering [31].

In practice, to maximize meter performance, measurement pickups are placed near the antinodes of the antisymmetric mode which is excited by the flow through Coriolis forces; for the present model that would be the maxima of $\varphi_{02}(x)$, i.e. $\Delta x=\frac{1}{4}$. For this case (42)–(45) gives the phase shift, meter sensitivity, and zero shift, respectively,

$$\Delta\psi(\tfrac{1}{4}) = s_1(\tfrac{1}{4})(\alpha v+\tfrac{3}{16}\beta_2),$$

$$s_1\left(\frac{1}{4}\right)=\frac{32\sqrt{2}}{45\pi^2}(1+r_{1,1/4}\kappa_1),\quad r_{1,1/4}=2\left(1+\frac{4}{15\pi}\right)-\frac{1}{\sqrt{2}}\approx 1.463,$$

$$\Delta\psi_0(\tfrac{1}{4})=\tfrac{3}{16}\beta_2 s_1(\tfrac{1}{4}), \tag{46}$$

which we recall is an approximation, supposed to be correct up to second order, i.e. it neglects terms of cubic order and smaller in the parameters assumed to be small. This also implies that the second term in the expression for s_1 in (46) should be small compared to unity. As an example one could consider this term "small" if order of magnitude 1/10 or smaller. This would imply $\kappa_1=\kappa_{u0}+\kappa_{ul}$ should be $O(\frac{1}{10}/r_{1,1/4})=O(0.1)$, which by the definition of $\kappa_{u0,l}$ in (4) means that for (46) to be a reasonable approximation, the transverse deflections at each flexible support should not exceed about $\frac{1}{2}\times 0.1=5\%$ of the mid-pipe deflection, for a given transverse mid-pipe load.

On the assumed smallness of parameters, and according to (43), the quantities s_1, $\Delta\psi$, and $\Delta\psi_0$ vary smoothly and monotonically with all parameters for values of Δx near 1/4; therefore the particular choice $\Delta x=\frac{1}{4}$ is not critical for the analysis.

For parameters corresponding to an ideal system, a result identical to (46) (but with $\kappa_1=\beta_2=0$) was obtained by the authors by using the Rayleigh–Schrödinger variant [26] of the Lindstedt–Poincaré perturbation method.

In Section 5 we use the simple analytical prediction (46) to illustrate the effect of some imperfections on flowmeter key factors, comparing also to the results of pure numerical analysis of the original system (1)–(3), i.e. without any assumptions on the smallness of parameters. As the assumptions underlying the approximate analysis become better fulfilled, i.e. when the parameters assumed small are decreased in magnitude, then increasingly accurate agreement with the numerical solution should be, and is, observed. The following section describes how the numerical analysis was performed.

4. Primary resonant response II: numerical solution using Galerkin expansion

Using instead a standard Galerkin approach to discretize the equation of motion (1) directly, we expand the unknown solution $u(x,t)$ into

$$u(x,t)=\sum_{j=1}^{N} q_j(t)\varphi_j(x), \tag{47}$$

where $\varphi_j(x)$, $j=1,\ldots,N$, are suitable expansion functions satisfying all boundary conditions of the problem, and $q_j(t)$ the new set of independent variables.

4.1. Expansion functions

For the expansion functions φ_j we use the N lowest mode shapes of the corresponding unforced, undamped and uniform pipe with no flow, but with flexible supports (if $\kappa_{u0,l}\neq 0$). This set is both relatively simple, satisfies all boundary conditions (3) (by contrast to φ_{0j} as defined by (11) and (12)), and is capable of capturing the dynamic response in the case of interest, i.e. primary 1st-mode resonance. To calculate φ_j, let, $p=L_k=L_\beta=\nu=0$ in (1), substitute $u=\varphi(x)e^{i\omega t}$ into (1) and (3) to obtain the eigenvalue problem $\varphi''''=\omega^2\varphi$ with boundary conditions $\varphi(0)+\varepsilon\pi^{-3}\kappa_{u0}\varphi'''(0)=\varphi''(0)=\varphi(1)-\varepsilon\pi^{-3}\kappa_{u1}\varphi'''(1)=\varphi''(1)=0$, and general solution $\varphi=\varphi_j$:

$$\varphi_j(x)=c_{1,j}\cosh(\gamma_j x)+c_{2,j}\sinh(\gamma_j x)+c_{3,j}\cos(\gamma_j x)+c_{4,j}\sin(\gamma_j x),\quad j=1,2,\ldots, \tag{48}$$

where $\gamma_j=\sqrt{\omega_j}$. Here the constants $c_{i,j}$, $i=1,\ldots,4$, $j=1,\ldots,N$, are determined by inserting (48) into the boundary conditions, giving for each j a homogeneous set of algebraic equations:

$$\mathbf{A}(\gamma)\mathbf{c}=\mathbf{0}, \tag{49}$$

where $\mathbf{c}=\{c_1\cdots c_4\}^{\mathrm{T}}$, and,

$$\mathbf{A}(\gamma)=\begin{bmatrix} 1 & 0 & -1 & 0\\ 1 & \tilde{\kappa}_{\gamma 0} & 1 & -\tilde{\kappa}_{\gamma 0}\\ \cosh\gamma & \sinh\gamma & -\cos\gamma & -\sin\gamma\\ \cosh\gamma-\tilde{\kappa}_{\gamma l}\sinh\gamma & \sinh\gamma-\tilde{\kappa}_{\gamma l}\cosh\gamma & \cos\gamma-\tilde{\kappa}_{\gamma l}\sin\gamma & \sin\gamma+\tilde{\kappa}_{\gamma l}\cos\gamma \end{bmatrix}, \tag{50}$$

where $\tilde{\kappa}_{\gamma 0,l}=\pi^{-3}\kappa_{u0,l}\gamma^3$. The requirement $|\mathbf{A}(\gamma)|=0$, which is necessary for non-trivial solutions $\mathbf{c}_j\neq\mathbf{0}$ to (49) to exist, gives a scalar nonlinear algebraic equation which can be solved numerically for $\gamma=\gamma_j$, $j=1,2,\ldots$, $\gamma_1<\gamma_2<\cdots<\gamma_N$, using, e.g. $\gamma_j=j\pi$ (i.e. the solution for the case of no support flexibility, $\kappa_{u0}=\kappa_{ul}=0$) as starting values for the iterations. This gives the corresponding natural frequencies $\omega_j=\gamma_j^2$ for free, undamped oscillations of the uniform pipe without flow, but taking into account support flexibility. Substituting any γ_j for γ in (49) and solving for $\mathbf{c}$ then gives the corresponding $\mathbf{c}_j$, which can be arbitrarily normalized, and determines the corresponding mode shape $\varphi_j(x)$ through (48).

4.2. Discretised system

Following the Galerkin procedure [32], one substitutes (47) into (1), multiplies by any $\varphi_i(x)$, and integrates over the pipe length to obtain

$$\mathbf{M}\ddot{\mathbf{q}}+\mathbf{C}\dot{\mathbf{q}}+\mathbf{K}\mathbf{q}=\mathbf{f}\cos(\Omega t), \tag{51}$$

where $\mathbf{q}(t)=\{q_1(t)\cdots q_N(t)\}^T$ holds the modal coordinates, and the components (i,j) of the modal mass, stiffness, and damping matrix, and the modal force vector are, respectively,

$$\mathbf{M}_{ij}=\int_0^1 \varphi_i\varphi_j\,\mathrm{d}x;\quad \mathbf{K}_{ij}=\int_0^1 \varphi_i\varphi_j''''\,\mathrm{d}x+\varepsilon\left(\alpha v^2\int_0^1 \varphi_i\varphi_j''\,\mathrm{d}x+\int_0^1 \varphi_i L_k\varphi_j\,\mathrm{d}x\right),$$

$$\mathbf{C}_{ij}=\varepsilon\left(2\alpha v\int_0^1 \varphi_i\varphi_j'\,\mathrm{d}x+\int_0^1 \varphi_i L_\beta\varphi_j\,\mathrm{d}x\right);\quad \mathbf{f}_i=\varepsilon p\varphi_i(x_p),\quad i,j=1,\ldots,N. \tag{52}$$

Eq. (51) then forms a system of ordinary differential equations, governing time evolution of the modal coordinates $q_j(t)$.

4.3. Excitation condition of interest

The pipe is assumed to be excited resonantly in its fundamental symmetric mode. The resonance frequency of this mode changes with fluid flow, with support flexibility, and with other imperfections. It can be calculated by letting $\mathbf{f}=\mathbf{0}$ in (51), insert a time harmonic solution $\mathbf{q}(t)=\boldsymbol{\varphi}^* e^{\lambda t}$, and solve the resulting algebraic eigenvalue problem numerically for the fundamental eigenvalue λ_1. If the flow speed v is nonzero, or if $\mathbf{C}$ is not proportional to $\mathbf{K}$ or $\mathbf{M}$, then for small damping the eigenvalues $\lambda=\lambda_j$ come as complex conjugate pairs, with their imaginary parts ω_j^* defining the jth natural frequency, and the real part d_i defining the damping ratio $\zeta_j=\mathrm{d}_j/\omega_j^*$ of mode j. Thus, as the excitation frequency for resonant excitation of the fundamental mode we take $\Omega=\omega_1^*=\mathrm{Im}(\lambda_1)$.

4.4. Resonant 1st-mode response

The stationary response under resonant excitation of the fundamental mode is obtained by substituting a harmonic solution form:

$$\mathbf{q}(t)=\mathbf{a}\sin(\Omega t)+\mathbf{b}\cos(\Omega t), \tag{53}$$

into (51). Separating the in-phase ($\cos(\Omega t)$) and out-of-phase ($\sin(\Omega t)$) terms then gives

$$\begin{bmatrix}\mathbf{K}-\Omega^2\mathbf{M} & -\Omega\mathbf{C}\\ \Omega\mathbf{C} & \mathbf{K}-\Omega^2\mathbf{M}\end{bmatrix}\begin{Bmatrix}\mathbf{a}\\ \mathbf{b}\end{Bmatrix}=\begin{Bmatrix}0\\ \mathbf{f}\end{Bmatrix}, \tag{54}$$

which can be solved for the vectors $\mathbf{a}$ and $\mathbf{b}$ to give the corresponding $\mathbf{q}$(t) for any excitation frequency Ω, including the particular 1st-mode resonance frequency $\Omega=\omega_1^*$ of interest here.

4.5. Phase shift between two pipe points under resonant 1st-mode response

Substituting $\Omega=\omega_1^*$ into (53) and (54) and solving (54) for the corresponding resonant values of $\mathbf{a}(t)=\{a_1(t)\cdots a_N(t)\}^T$ and $\mathbf{b}(t)=\{b_1(t)\cdots b_N(t)\}^T$, the resulting $\mathbf{q}$ can be substituted into (47) to give, when rewriting from sine–cosine to amplitude-phase form:

$$u(x,t)=A(x)\sin(\Omega t-\psi(x)), \tag{55}$$

where the amplitude A and the phase ψ generally vary along the pipe axis x:

$$A(x)=\sqrt{\Big(\sum_{j=1}^{N}(a_j\varphi_j(x))\Big)^2+\Big(\sum_{j=1}^{N}(b_j\varphi_j(x))\Big)^2}, \tag{56}$$

$$\psi(x)=-\arctan\Big(\sum_{j=1}^{N}b_j\varphi_j(x)/\sum_{j=1}^{N}a_j\varphi_j(x)\Big). \tag{57}$$

Eq. (57) can be used to calculate the phase shift $\Delta\psi=\psi(x_1)-\psi(x_2)$ between any two pipe points. For two symmetrically situated points $x_{1,2}=\frac{1}{2}\mp\Delta x$ this gives

$$\Delta\psi(\Delta x)=\psi(\tfrac{1}{2}-\Delta x)-\psi(\tfrac{1}{2}+\Delta x), \tag{58}$$

which can be compared to the corresponding phase shift predicted by the simple analytical approximations, e.g. (46), which holds for $\Delta x=\frac{1}{4}$.

Eqs. (58) with (57) will be subsequently referred to as the *numerical solution*; it was implemented using MATLAB. Convergence of numerically calculated phase shifts $\Delta\psi$ with increased number of included modes N was tested in each of the cases reported in Section 5 below. In general $N=2$ was found to capture the main part of the phase shift, while $N=4$ gave a small correction to that, and $N>4$ only marginal changes; in most cases $N=8$ was used.

The numerical solution can be expected to offer good accuracy as N is increased, converging towards the exact solution as $N\to\infty$. It does not require imperfections to be small, but on the other hand provides very little insight into how imperfections affect phase shift. The numerical solution is thus complementary to the analytical solution (46), which is approximate and assumes imperfections to be small, but offers direct insight into how these imperfections affect phase shift. Thus the key role of numerical solution is here to test the quality of analytical solutions. For parameter ranges where the analytical expressions can be validated, these are considered more useful than numerical solutions for practical innovation, design and troubleshooting.

5. Application examples: effects of imperfections

The simple prediction (46) is here used to illustrate the effect of some imperfections on flowmeter key factors, recalling from Section 2 that the ideal pipe has no transverse or rotational damping ($\beta_u=\beta_\theta=0$), no transverse flexibility at either support end ($\kappa_{u0}=\kappa_{ul}=0$), and no inhomogeneity in transverse or flexural stiffness ($k_u=k_\theta=0$). For the numerical examples we use a mass ratio of $\alpha=0.3$ and a mass flow range $\alpha v\in[0;\ 0.1]$, roughly corresponding to a specific industrial Coriolis flowmeter measuring water flow from zero to full nominal flow rate. Unless otherwise stated the pipe damping is taken to be axially uniform with $\beta_u(x)=0.002$; this corresponds to a quality factor $Q=\omega_1/\beta_u\approx 5000$ for the drive mode, or a damping ratio of $(2Q)^{-1}\approx 0.01$ percent.

5.1. Effect of rotational damping at supports, $\beta_\theta(x)\neq 0$

In this case the pipe is ideal except for the presence of rotational damping at the simple supports, i.e. $\beta_u=\kappa_{u0}=\kappa_{ul}=k_u=k_\theta=0$, but $\beta_\theta(x)\neq 0$ at $x=0$ or 1. Specifically we let

$$\beta_\theta(x)=\beta_{\theta 0}\delta(x)+\beta_{\theta l}\delta(x-1), \tag{59}$$

where $\delta(x)$ is Dirac's delta function, and $\beta_{\theta 0}$ and $\beta_{\theta l}$ are the coefficients of linear rotational damping at the left and right pipe support, respectively. Using (27) and (29) gives

$$\kappa_1=\kappa_2=k_1=k_2=0,\quad K_1=\tfrac{1}{2}\alpha v^2,\quad \beta_1=2\pi^2(\beta_{\theta 0}+\beta_{\theta l}),\quad \beta_2=4\pi^2(\beta_{\theta 0}-\beta_{\theta l}), \tag{60}$$

so that β_1 and β_2 express, respectively, the magnitude and the asymmetry in rotational support damping. Using (46) one obtains the predicted phase shift, sensitivity, and zero shift, respectively,

$$\Delta\psi\left(\frac{1}{4}\right)=s_1\left(\frac{1}{4}\right)\left(\alpha v+\frac{3}{4}\pi^2(\beta_{\theta 0}-\beta_{\theta l})\right),\quad s_1\left(\frac{1}{4}\right)=\frac{32\sqrt{2}}{45\pi^2}\approx 0.1,\quad \Delta\psi_0\left(\frac{1}{4}\right)=\frac{8}{15}(\beta_{\theta 0}-\beta_{\theta l}), \tag{61}$$

which implies that:

(a) Small rotational damping at the supports does not necessarily cause phase shift, but any *asymmetry* ($\beta_{\theta 0}-\beta_{\theta l}\neq 0$) in support damping causes a phase shift proportional to the asymmetry.
(b) The phase shift caused by fluid mass flow αv is inseparable from the phase shift caused by damping asymmetry, unless either the mass flow or the damping asymmetry is known, or known to be constant in time. This can be understood also in terms of the corresponding forces involved: The forces of rotational support damping are proportional to the angular velocity $\dot{u}'$ of pipe segments, just as are the Coriolis forces corresponding to mass flow.
(c) The effect of rotational support damping can be of the same order of magnitude as the effect of mass flow. This occurs when the (nondimensional) damping asymmetry is similar in magnitude to the mass flow, a situation more likely to arise at low values of flow speed.
(d) Damping asymmetry causes a phase shift $\Delta\psi_0\neq 0$ even at zero fluid flow ($\alpha v=0$). This zero shift can be compensated for during initial meter calibration. However, during later operation the support damping may fluctuate in time and (asymmetrically) in space due to many factors, e.g. temperature, wear, lubrication, or vibration level—in any case causing phase shifts that will read out as equivalent changes in mass flow. Thus, fluctuating support damping could be a factor contributing to the lack of *zero-point stability* occasionally observed with industrial Coriolis flowmeters, referring to changes in meter readings under (allegedly) constant mass flow.

Fig. 2 shows the variation in phase shift $\Delta\psi(\frac{1}{4})$ with mass flow αv for five values of asymmetry ($\beta_{\theta 0}-\beta_{\theta l}$) in rotational support damping. The middle of the five lines is for symmetric damping, the top and bottom lines for a level of support damping asymmetry (positive and negative) five time as large as the transverse damping β_u of the pipe, and the two middle-most lines for an asymmetry of half the magnitude of the pipe damping. As appears the analytical approximation (61) (lines) rather accurately agrees with the numerical solution (57) and (58) (symbol markers). Good accuracy of the

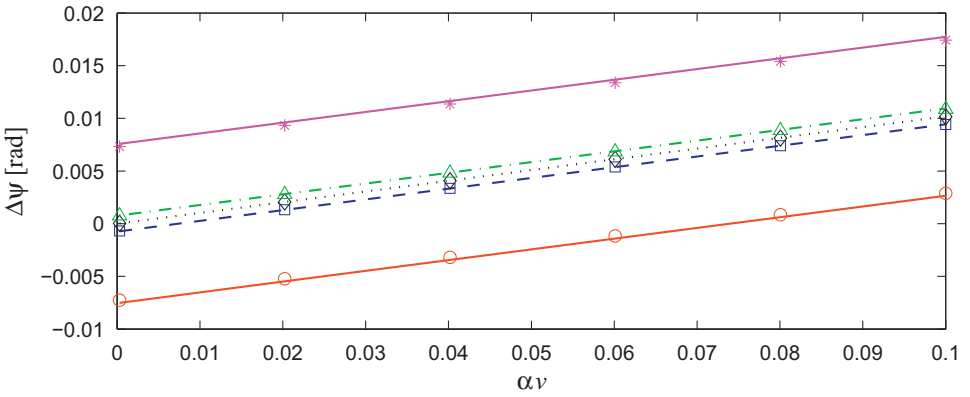

Fig. 2. Effect of rotational support damping ($\beta_{\theta 0}$,$\beta_{\theta l}$) on phase shift $\Delta\psi(\frac{1}{4})$ for varying mass flow $\alpha\nu$, as obtained by the analytical approximation (61) (lines), and by a numerical solution (57) and (58) to (1)–(3) using N=8 modes (symbol markers). The total support damping is $\beta_{\theta 0}+\beta_{\theta l}=10^{-2}$, and from bottom to top the lines show $\Delta\psi(\frac{1}{4})$ for different levels of damping asymmetry, $\beta_{\theta 0}-\beta_{\theta l}=\{-10^{-2},-10^{-3},0,+10^{-3},+10^{-2}\}$. Other parameters: α=0.3, $p=10^{-3}$, β_u=0.002, $\kappa_{u0}=\kappa_{ul}=\beta_\theta=k_u=k_\theta=0$.

analytical approximation persists even if both the magnitude and asymmetry in rotational damping is raised to as much as about 0.3, i.e. to levels of damping far above physically realistic values. Hence the simple expression (61) gives about the same accuracy as the numerical solution, but provides much more insight. The agreement between analytical and numerical results can become even closer by reducing the number of modes used in the numerical Galerkin expansion to N=2; however, this just reflects that the analytical approximation relies on only the two lowest modes. Using N=6, 8, or 10 for computing Fig. 2 produced no discernible changes to the plot, but increased computational time almost in proportion to N^4 ({122, 362, 855} s for $N=\{6, 8, 10\}$ on a 2.4 GHz 2CPU PC).

Fig. 2 also illustrates some of the general observations (a–d) made above from (61): A zero shift is noted (phase shift even for zero mass flow) which grows with the damping asymmetry, while the sensitivity is not affected by this asymmetry (all the lines are parallel).

5.2. *Effect of rotational stiffness at supports, $k_\theta(x)\neq 0$*

Here the pipe is ideal except for a small but finite rotational stiffness at the hinged supports, i.e. $\beta_u=\beta_\theta=k_u=\kappa_{u0}=\kappa_{ul}=0$ but $k_\theta(x)\neq 0$ at x=0 or 1, specifically

$$k_\theta(x)=k_{\theta 0}\delta(x)+k_{\theta l}\delta(x-1), \tag{62}$$

where, $k_{\theta 0}$ and $k_{\theta l}$ are the stiffness coefficients of linear rotational springs at the pipe ends. Using (27) and (29) gives

$$\kappa_1=\kappa_2=\beta_1=\beta_2=0,\quad K_1=\tfrac{1}{2}\alpha\nu^2-\tfrac{1}{2}k_1,\quad k_1=2(k_{\theta 0}+k_{\theta l}),\quad k_2=4(k_{\theta 0}-k_{\theta l}), \tag{63}$$

so that k_1 and k_2 express, respectively, the total magnitude and the asymmetry in rotational support stiffness. Then (46) gives

$$\Delta\psi\left(\frac{1}{4}\right)=s_1\left(\frac{1}{4}\right)\alpha\nu,\quad s_1\left(\frac{1}{4}\right)=\frac{32\sqrt{2}}{45\pi^2},\quad \Delta\psi_0\left(\frac{1}{4}\right)=0, \tag{64}$$

which is the same as for an ideal pipe. This implies that:

(e) Small rotational support stiffness has no effect on measured phase shift, to the order of accuracy used in the approximation. If there is an effect, it must be of cubic or smaller order in the parameters assumed small (cf. remark below (46)), and thus at least two orders of magnitude smaller than the primary effect of mass flow $\alpha\nu$. For practical purposes this can be considered negligible, or overshadowed by the effects of other imperfections.

(f) Though not affecting phase shift, rotational support stiffness still affect pipe vibrations to first order, as predicted by (32) and (33), where a nonzero value of k_2 (i.e. asymmetric support stiffness) increases the amplitude of the second vibration mode φ_{02}. The reason this does not cause phase shift is that k_2 appears in the part of the response which is in phase with the driving force (at least when, as here, rotational support damping is neglected, so that $\beta_1=\tilde{\eta}_{01}=0$, cf. (32)–(34)).

(g) Consideration to the effect of rotational stiffness on phase shift should go instead to the *damping* accompanying any real structure having finite stiffness, cf. Section 5.1.

A plot of phase shift versus mass flow for this case, using the same base parameters as for Fig. 2 and $k_{\theta 0}+k_{\theta l}$=0.1, $k_{\theta 0}-k_{\theta l}=[-10^{-1},-10^{-2},0,+10^{-2},+10^{-1}]$ appears trivial and is thus not shown; it is similar to Fig. 2, except that all the

lines collapse into the middle line in Fig. 2 (since the analytical prediction does not depend on rotational stiffness). Also here the agreement with numerical analysis is good, in the sense that magnification of parts of the figure is necessary to see that numerical analysis gives slightly different phase shifts for the different values of rotational stiffness. The relative deviations between analytically and numerically obtained phase shifts are in the range $10^{-2}-10^{-4}$ for this example.

5.3. Effect of transverse flexibility at supports, $\kappa_{u0}+\kappa_{ul}\neq 0$

This pipe is ideal, except for the presence of a small transverse flexibility at the (then only approximately) simple supports, i.e. $\beta_u=\beta_\theta=k_u=k_\theta=0$, but $\kappa_{u0}+\kappa_{ul}\neq 0$. By (27)–(29)

$$\kappa_1=\kappa_{u0}+\kappa_{ul},\quad \kappa_2=\kappa_{u0}-\kappa_{ul},$$

$$k_1=k_2=\beta_1=\beta_2=0,\quad K_1=\tfrac{1}{2}\alpha v^2+\pi\kappa_1, \tag{65}$$

so that κ_1 and κ_2 expresses, respectively, the total magnitude and the asymmetry in transverse support flexibility. With (46) the predicted phase shift becomes

$$\Delta\psi\left(\frac{1}{4}\right)=s_1\left(\frac{1}{4}\right)\alpha v,\quad s_1\left(\frac{1}{4}\right)=\frac{32\sqrt{2}}{45\pi^2}(1+r_{1,1/4}(\kappa_{u0}+\kappa_{ul})),\quad \Delta\psi_0\left(\frac{1}{4}\right)=0, \tag{66}$$

with the number constant $r_{1,1/4}$ defined in (46). According to this prediction:

(h) Transverse support flexibility increases the meter sensitivity s_1, but does not affect phase shift at zero mass flow, i.e. there is no zero shift.
(i) The increase in sensitivity is proportional to the summed transverse support flexibility, and is thus present even in the case of purely symmetrical support flexibility.
(j) The effect of transverse support flexibility on phase shift is of second order (proportional to the product of the two small terms κ_1 and αv), and thus of lower order than the effect of mass flow αv.

Fig. 3(a) illustrates the variation of phase shift with mass flow for three levels of equal flexibility $\kappa_{u0}=\kappa_{ul}$ of the two supports in the range 10^{-3}–10^{-1}. The lowest line (dotted) is for the smallest support flexibility 10^{-3}, i.e. the pipe is very close to being simply supported and this curve is almost identical to the one for an ideal pipe (i.e. the middle line in Fig. 2, dotted). The analytical approximation (66) (lines) agrees well with the numerical solutions (57) and (58) (symbol markers), with minor discrepancies seen only for the largest support flexibility 10^{-1}. Fig. 3(a) also illustrates some of the general

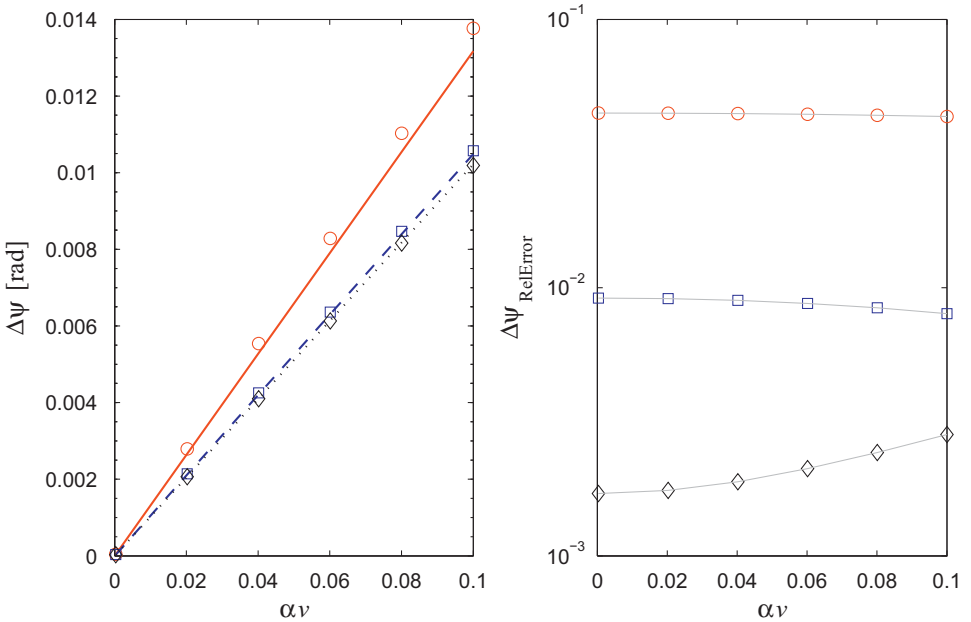

Fig. 3. (a) Effect of transverse support flexibility (κ_{u0},κ_{ul}) on phase shift $\Delta\psi(\frac{1}{4})$ for varying mass flow αv, as obtained by the analytical approximation (66) (lines), and by the numerical solution (57) and (58) to (1)–(3) using N=8 modes (symbol markers). The three sets of data are for $\kappa_{u0}=\kappa_{ul}=\{10^{-1},10^{-2},10^{-3}\}$ in, respectively, solid line/circles; dashed line/squares; and dotted line/diamonds. Other parameters as for Fig. 2; (b) relative deviation between analytical prediction and numerical analysis for the data shown in (a), with symbol markers defined as for (a).

observations (h–j) made above from (66), i.e. there is no zero shift, but an increase in sensitivity (line slope) with support flexibility.

Fig. 3(b) shows how the relative deviation between analytical prediction and numerical analysis decreases as the support flexibility becomes smaller, i.e. as the assumptions for the perturbation analysis is better met. This deviation can be perceived as the approximation error accompanying the perturbation analysis; its order of magnitude appears to match that of the support flexibility itself, e.g. for $\kappa_{u0}=\kappa_{ul}=10^{-2}$, the error is also of order magnitude 10^{-2}.

5.4. Effect of transverse damping at flexible supports, $\beta_u(x)\neq 0$

Transverse support flexibility (cf. Section 5.3) opens an additional pathway for energy dissipation, to be examined here. We consider $\beta_\theta=k_u=k_\theta=0$, but $\kappa_{u0}+\kappa_{ul}\neq 0$ (since to dissipate energy the supports need to move, i.e. they should be flexible), and $\beta_u(x)\neq 0$, in particular:

$$\beta_u(x)=\beta_{u0}\delta(x)+\beta_{ul}\delta(x-1), \tag{67}$$

where β_{u0} and β_{ul}, respectively, are the coefficients of linear transverse damping at the left and right pipe support. Using (27) and (29) still gives $\beta_1=\beta_2=0$, even if $\beta_u(x)\neq 0$, and thus (65) holds also for this case. Then (46) also gives (66) unchanged, and it follows that:

(k) Transverse damping of the flexible supports of the model, even if unsymmetrical, does not affect phase shift, at least not to the order of approximation employed.

The reason for this is that the transverse damping forces at the supports are of second order in the small parameters, occurring as a product of damping coefficients $\beta_{u0,l}$ which are small, and rigid body modes $\varphi_{10j}(x)$ which are also small (due to small support flexibility). This is a marked difference to the effect of *rotational* support damping, cf. Section 5.1, where the damping forces are proportional to first powers of the small parameters, and thus can have a similar influence on phase shift as mass flow.

Numerical simulation in this case gives results virtually indistinguishable from those already presented in Section 5.3 and Fig. 3(a) (top line and circle markers). This confirms the prediction in (k) above, i.e. for estimating the effect of transverse support flexibility on phase shift, the effect of energy dissipation is ignorable compared to that of mass flow and flexibility itself.

6. Conclusions

We have demonstrated how phase shift effects for vibrating fluid-conveying pipes with small imperfections can be conveniently analyzed using perturbation analysis. The results come as simple analytical expressions, relating measures of imperfection to vibration parameters of interest, such as the spatial phase shift relevant for Coriolis flowmeters. The analytical predictions provide immediate insight into which imperfections affect phase shift, and in which manner. Representative examples were tested against pure numerical solution, demonstrating very good agreement with analytical predictions.

Some general results were derived for imperfections associated with pipe supports. For example it was predicted, and validated numerically, that the asymmetric part of rotational support damping changes the spatial phase shift along the pipe in the same manner as does mass flow, so that—in a phase shift measuring flowmeter—any asymmetric fluctuation in rotational support damping could be mistaken for a change in mass flow. Similarly, a small flexibility at pipe supports supposed to be ideally rigid was shown to increase the ratio of phase shift to mass flow, thus changing the sensitivity for a Coriolis flowmeter. On the other hand, imperfections such as small transverse damping at flexible supports (even if asymmetric), or finite rotational stiffness at simple supports, were demonstrated to influence phase shift at a level proportional to the square product of small parameters, i.e. ignorable for typical applications.

The results were derived for a simple model of single straight pipe with uniform plug flow. This model ignores substantial features of real systems, e.g. industrial Coriolis flowmeters typically have two curved pipes, with clamped rather than simple supports, and are further influenced by, e.g. connected sensors and actuators, external disturbances, and non-uniform flow. However, the main physical properties could be unaffected by this seeming complexity, so that predictions based on simplified models (e.g. that phase grows linearly with the asymmetric part of the damping) could be used for creating hypotheses to be tested with detailed computational models, e.g. FEM and CFD models taking into account two-way fluid-structure interaction, or real laboratory experiments. If passing such tests with acceptable accuracy, the simple analytical predictions may be more valuable for applications than detailed numerical simulation, which are still highly time consuming and prohibits any deeper insight into the effects at play.

The combination of simple modeling and systematic perturbation analysis, used here for examining pipe support imperfections, can be readily extended to other kinds of imperfection. With the perturbation analysis used in Section 3, even consideration to weak nonlinearity is rather straightforward. Effects of imperfections in the form of weak nonlinearity, pulsating flow, and general non-proportional damping are currently investigated and partly reported [22,25].

Acknowledgments

The second author was supported by the Danish Agency for Science, Technology and Innovation, and by Siemens Flow Instruments A/S.

References

[1] C. Stack, R. Garnett, G. Pawlas, *A finite element for the vibration analysis of a fluid-conveying Timoshenko beam*, AIAA Technical Paper 93-1552-CP, 10pp, 1993.
[2] T. Wang, R.C. Baker, Y. Hussain, An advanced numerical model for single straight tube Coriolis flowmeters, *Journal of Fluids Engineering* 128 (2006) 1346–1350.
[3] R. Cheesewright, C. Clark, A. Belhadj, Y.Y. Hou, The dynamic response of Coriolis mass flow meters, *Journal of Fluids and Structures* 18 (2003) 165–178.
[4] M.P. Païdoussis, The canonical problem of the fluid-conveying pipe and radiation of the knowledge gained to other dynamics problems across applied mechanics, *Journal of Sound and Vibration* 310 (2008) 462–492.
[5] M.P. Païdoussis, *Fluid Structure Interactions: Slender Structures and Axial Flow*, Vol. 1, Academic Press, London, 1998.
[6] M. Anklin, W. Drahm, A. Rieder, Coriolis mass flowmeters: overview of the current state of the art and latest research, *Flow Measurement and Instrumentation* 17 (2006) 317–323.
[7] J. Hemp, J. Kutin, Theory of errors in Coriolis flowmeter readings due to compressibility of the fluid being metered, *Flow Measurement and Instrumentation* 17 (2006) 359–369.
[8] T.J. Cunningham, Zero shifts due to non-proportional damping, in: *Proceedings of the 15th International Modal Analysis Conference*, *IMAC*, Vol. 1, Coriolis flowmeter; damping; imperfection, 1997, pp. 237–243.
[9] J. Kutin, I. Bajsic, An analytical estimation of the Coriolis meter's characteristics based on modal superposition, *Flow Measurement and Instrumentation* 12 (2002) 345–351.
[10] R. Cheesewright, A. Belhadj, C. Clark, Effect of mechanical vibrations on Coriolis mass flow meters, *Journal of Dynamic Systems, Measurement, and Control* 125 (2003) 103–113.
[11] J. Kutin, I. Bajsic, Stability-boundary effect in Coriolis meters, *Flow Measurement and Instrumentation* 12 (2001) 65–73.
[12] J. Kutin, G. Bobovnik, J. Hemp, I. Bajsic, Velocity profile effects in Coriolis mass flowmeters: recent findings and open questions, *Flow Measurement and Instrumentation* (2006) 349–358.
[13] C. Rao, S. Mirza, A note on vibrations of generally restrained beams, *Journal of Sound and Vibration* 130 (1989) 453–465.
[14] A. Guran, R. Plaut, Stability boundaries for fluid-conveying pipes with flexible support under axial load, *Archive of Applied Mechanics* 64 (1994) 417–422.
[15] K. Chellapilla, H. Simha, Critical velocity of fluid-conveying pipes resting on two-parameter foundation, *Journal of Sound and Vibration* 302 (2007) 387–397.
[16] F. Kassubek, J. Gebhardt, R. Friedrichs, S. Keller, Influence of boundary conditions on Coriolis flowmeter measurement, *VDI Berichte* (2004) 281–288.
[17] H. Raszillier, F. Durst, Coriolis-effect in mass flow metering, *Archive of Applied Mechanics* 61 (1991) 192–214.
[18] N.M. Keita, Contribution to the understanding of the zero shift effects in Coriolis mass flowmeters, *Flow Measurement and Instrumentation* 1 (1989) 39–43.
[19] J. Dahl, J.J. Thomsen, Phase shift effects for fluid conveying pipes with non-ideal supports, in: *CD-ROM Proceedings of ICTAM 2008* (*International Congress of Theoretical and Applied Mechanics*), 2pp, Adelaide, Australia, 2008.
[20] U. Lange, A. Levient, T. Pankratz, H. Raszillier, Effect of detector masses on calibration of Coriolis flowmeters, *Flow Measurement and Instrumentation* 5 (1994) 255–262.
[21] G. Sultan, J. Hemp, Modelling of the Coriolis mass flowmeter, *Journal of Sound and Vibration* 132 (1989) 473–489.
[22] J.J. Thomsen, J. Dahl, N. Fuglede, S. Enz, Predicting phase shift of elastic waves in pipes due to fluid flow and imperfections, in: M.R. Pawelczyk, D. Bismor (Eds.), *Proceedings of the 16th International Congress on Sound and Vibration* (*ICSV16*), 8pp, Kraków, Poland, International Institute of Sound and Vibration, 2009.
[23] R. Cheesewright, C. Clark, D. Bisset, The identification of external factors which influence the calibration of Coriolis massflow meters, *Flow Measurement and Instrumentation* 11 (2000) 1–10.
[24] R. Cheesewright, C. Clark, Y.Y. Hou, The response of Coriolis flowmeters to pulsating flows, *Flow Measurement and Instrumentation* 15 (2004) 59–67.
[25] S. Enz, J.J. Thomsen, Phase shift effects for vibrating pipes conveying pulsating fluid, in: *Proceedings of the Seventh EUROMECH Solid Mechanics Conference* (*ESMC2009*), 2pp, Lisbon, Portugal, 2009.
[26] A.H. Nayfeh, *Perturbation Methods*, Wiley, New York, 1973.
[27] A.H. Nayfeh, D.T. Mook, *Nonlinear Oscillations*, Wiley, New York, 1979.
[28] J.K. Kevorkian, J.D. Cole, *Multiple Scale and Singular Perturbation Methods*, Springer, New York, 1996.
[29] J.J. Thomsen, *Vibrations and Stability: Advanced Theory, Analysis, and Tools*, Springer, Berlin, Heidelberg, 2003.
[30] A.H. Nayfeh, S.J. Serhan, Response statistics of non-linear systems to combined deterministic and random excitations, *International Journal of Non-Linear Mechanics* 25 (1990) 493–509.
[31] R.C. Baker, *Flow Measurement Handbook*, Cambridge University Press, Cambridge, 2000.
[32] A.A. Shabana, *Vibration of Discrete and Continuous Systems*, second ed., Springer, New York, 1997.